Air Trench Bends and Splitters for Dense Optical Integration in Low Index Contrast

Shoji Akiyama, *Student Member, IEEE*, Miloš A. Popović, *Student Member, IEEE*, Peter T. Rakich, Kazumi Wada, Jürgen Michel, Hermann A. Haus, *Life Fellow, IEEE, Fellow, OSA*, Erich P. Ippen, *Fellow, IEEE, Fellow, OSA*, and Lionel C. Kimerling, *Member, IEEE*

***Abstract*—Low-loss air trench structures that permit reduced-size bends in low (Δ = 0.7–7%) and medium (Δ = 7–20%) index contrast waveguides are demonstrated. Local high index contrast at bends is achieved by introducing air trenches with "cladding tapers" that provide an adiabatic mode transition between low and high index contrast regions. We have fabricated and measured the performance of bends and T-splitters in silica low index contrast waveguides. Complimentary metal–oxide–semiconductor (CMOS) compatible processes are effective in processing, and measured losses are low and consistent with theoretical simulations.**

***Index Terms*—Air trench bend, bend loss, cladding taper, enhanced lateral mode confinement, low index contrast, silica waveguide.**

I. Introduction

THE low index contrast silica bench technology that is often referred to as planar lightwave circuit (PLC) or silica optical bench (SiOB) has been widely used in the fabrication of passive integrated optical components such as arrayed waveguide gratings [1]. It is well known that PLC (or SiOB) structures provide low fiber-to-chip coupling and low propagation losses due to their low index contrast between core and cladding. A major drawback of PLC (or SiOB) technology is a relatively large footprint, where a critical factor is the minimum waveguide bend radius. Due to weak light confinement, low index contrast waveguide circuits require large bend radii, ranging from millimeters to a centimeter ($\Delta = 0.25$–1.5%) [1], to reduce radiative loss. On the other hand, high index contrast material systems such as Si/SiO_2, where the index difference is as much as 2, offer dense integration but pose challenges in fiber-to-chip coupling and scattering loss from sidewall roughness.

Air trench (AT) waveguide sections provide a drastic reduction in the bend radius while permitting simple fabrication. By eliminating this scaling limitation, AT design allows large-scale optical integration to be achieved on low and medium index contrast platforms.

Manuscript received April 26, 2004; revised April 18, 2005. This work was supported by the MRSEC Program of the National Science Foundation under Award No. DMR 02-13282.

S. Akiyama, K. Wada, J. Michel, and L. C. Kimerling are with the Department of Materials Science and Engineering, Massachusetts Institute of Technology, Cambridge, MA 02139 USA (e-mail: akiyama@alum.mit.edu).

M. A. Popović, P. T. Rakich, H. A. Haus, and E. P. Ippen are with the Research Laboratory of Electronics, Massachusetts Institute of Technology, Cambridge, MA 02139 USA.

Digital Object Identifier 10.1109/JLT.2005.850047

II. Background

Bend loss is a fundamental performance property of dielectric waveguide circuits. Radiative loss at bends decreases with bend radius [2]–[6] and with high index contrast. High index contrast seems the natural choice to achieve dense integration of optical components, but fabricated high index contrast waveguides suffer high propagation loss, caused by sidewall roughness of the waveguide [7], [8], and poor coupling between the fiber and the waveguide due to mode shape mismatch and alignment sensitivity. It was reported that propagation loss is proportional to the third power of the sidewall roughness [7], [8]. On the other hand, low index contrast waveguides provide small propagation loss and good coupling between fiber and waveguide but require relatively large bend radii to achieve low bend loss. This size problem is critical for the dense integration of optical components. Photonic crystal waveguides are attracting considerable attention as another candidate for dense optical integration [9]–[11], but due to poor vertical mode confinement and fabrication complexity, they have shown high propagation loss. Recently the use of medium index contrast waveguides has been proposed where the index difference ranges from $\Delta n = 0.05$–0.3 to avoid the problems of high index contrast and low index contrast waveguides [12]–[17]. But the bend radius is still a problem for dense integration. For example, when the index difference is $\Delta n = 0.1$ ($\Delta = 6.8\%$), a 100- to 200-μm radius is required to achieve 98% transmission (0.09 dB loss) in one 90° turn. Thus, the density of integration in low-to-medium index contrast using conventional waveguides is limited by bend loss.

We have recently proposed a new scheme using air trenches to provide locally enhanced lateral confinement to enable small bends and T-splitters [18]. We use adiabatic tapering to avoid abrupt junction-induced mode mismatch and Fresnel reflection. Optical waveguide bends are thus miniaturized while preserving low-loss performance. The basic configuration of an AT bend is depicted in Fig. 1.

III. Air Trench Bend Theory and Simulations

The theoretical details of AT bend design are discussed in [18]. Fig. 2 summarizes bend design for conventional waveg-

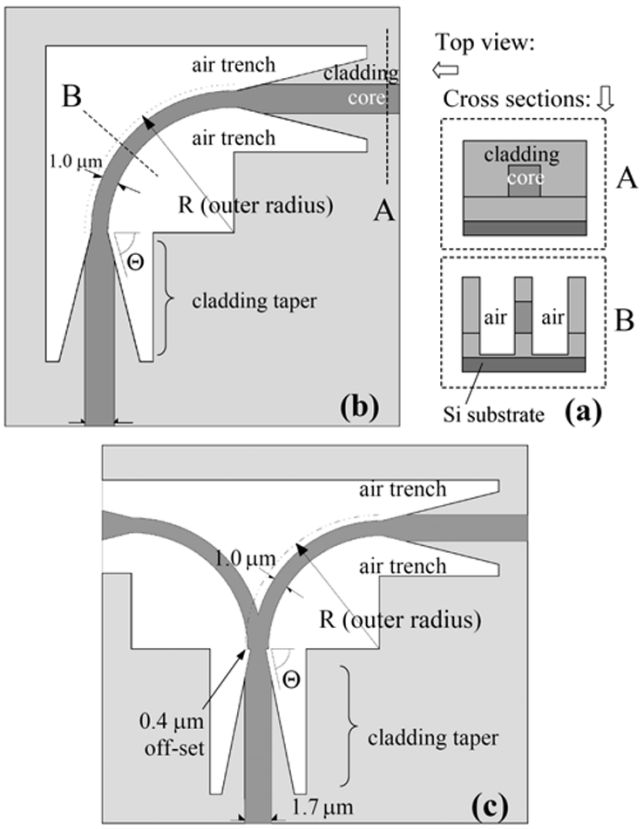

Fig. 1. Air trench design schematic. (a) Cross sectional view of (A) low index straight waveguide and (B) bend. (b) ATB. Outer radius $= 3.7$, 4.7, 6.2, 8.7, and 10.7 μm, and $\Theta = 55$, 65, 76, and 80°. (c) Air trench T-splitter schematic. $R = 10.7$ μm and $\Theta = 80°$.

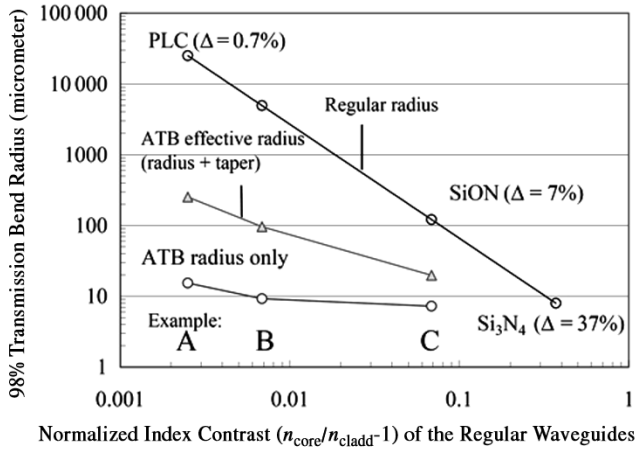

Fig. 2. Bend radius design plot. Normalized index contrasts (horizontal axis) denote those for regular (straight) waveguide sections. Local normalized index contrasts of air trench waveguides at bend sections $(n_{\rm core}/n_{\rm air} - 1)$ for examples A, B, and C are 0.448, 0.454, and 0.542, respectively. Claddings are assumed to be silicon dioxide (SiO_2). Radiation loss in regular and AT bends is evaluated numerically according to the approaches in [4] and [5] after the customary conformal transformation for bent waveguides [3]. The result is a theoretical reduction in bending radius by a factor of 10–1000 and in total bend structure edge length by a factor of 4–60.

uides and AT sections for the case of 0.09 dB loss, which corresponds to 98% transmission. Three examples (A, B, and C) depict the case where $\Delta(n_{\rm core}/n_{\rm cladding} - 1) = 0.25$, 0.68, and 6.8%, respectively. Radiation loss in regular and AT bends is evaluated numerically according to the approaches in [4] and [5] after the customary conformal transformation for bent waveguides [3]. The result is a theoretical reduction in bend radius by a factor of 10–1000 and in total bend structure edge length (bend + taper) by a factor of 4–60.

Fig. 1 summarizes the structural components of the AT design. In straight propagation, the structure is a simple low index contrast channel waveguide [cross section A in Fig. 1(a)]. At bends, air trenches are placed to enhance lateral mode confinement by introducing local high index contrast [cross section B in Fig. 1(a)]. To avoid junction loss between the straight and the bending sections, an adiabatic taper is placed at the input and output junctions. These adiabatic tapers provide fast mode transitions between straight and bending waveguides. This type of AT bend can result in a drastic reduction in bend radius depending on the index contrast between core and cladding.

IV. Design Parameters

For the fabrication of air trench bends (ATBs) and T-splitters, the waveguide index difference is targeted at $\Delta n = 0.1$ ($\Delta = 6.8\%$, example C in Fig. 2). Silicon oxynitride (SiON) was chosen as the core material because its refractive index can be easily adjusted during deposition just by changing the gas composition [17]. Radii (R) and linear taper angles (Θ) are varied from 3.7 to 10.7 μm and 55 to 80°, respectively, to provide a sensitivity analysis of the design parameters. In our notation, the outer radius of the channel waveguide was used as our definition of the radius because in our case, where the sharp bends are discussed, the mode behaves like a whispering gallery mode that is guided by the outer edge [18]. The widths of the channel and AT waveguides are 1.7 μm and 1 μm, respectively, to keep single-mode operation in the low index contrast (straight) and high index contrast (bend) regions. Trench depth was chosen to be 4 μm to minimize substrate loss. The trench depth should be more than twice as deep as the core thickness to ensure a maximum of 0.01 dB substrate loss [18]. This low loss is achieved by laterally confining the evanescent tail of guided in-between deep air trenches. For the T-splitter, the radius and the taper are fixed at 10.7 μm and 80°, respectively [Fig. 1(b)].

V. Fabrication

The fabrication process is schematically outlined in Fig. 3. All of the processes are complimentary metal–oxide–semiconductor (CMOS) compatible. The starting substrate was a 1-mm-thick Czochralski-grown p-type (0.1–100 Ωcm) silicon wafer, and the under cladding was grown by a high-pressure thermal oxidation process at 1050 °C [Fig. 3(a)]. The thickness of the under cladding was 16 μm. After growing the under cladding, a SiON core layer was deposited through the plasma enhanced chemical vapor deposition (PECVD) process [Fig. 3(b)]. The target index is 1.5456 at 1.55 μm so that the index difference between core and cladding is 0.1. SiON deposition was done using Novellus Concept1. The thickness and refractive index (at 633 nm) of the SiON film were 2.0498 μm and 1.5294, respectively,

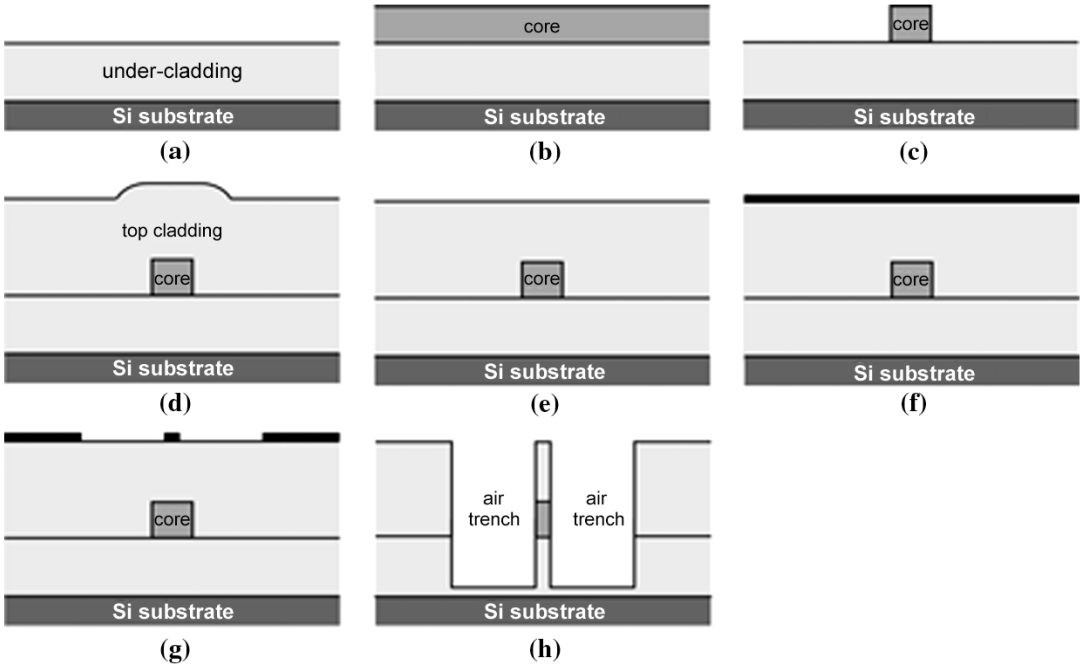

Fig. 3. Brief schematic of the ATB/T-splitter flow process (not to scale). All steps are done using conventional CMOS processes.

as deposited. This evaluation was done by a Metricon model 2010 prism coupler. The wavelengths used here were 633 and 1550 nm in transverse electric (TE) mode.

After core layer deposition, a high-temperature anneal (N_2 ambient, 1050 °C 1–6 h) was applied to consolidate the SiON film and to remove nitrogen–hydrogen covalent bonds that introduce absorption loss in the 1.55-μm wavelength range [12]. During the annealing process, the SiON layer refractive index and thickness change as shown in Fig. 4. Both the thickness and the refractive index converge to stable values after 4 h. We used SiON that had been annealed for 4 h for all the structures in this work.

Photolithography was done using a Nikon i-line (365 nm) stepper NSR-2205i9. The photoresist used here was Shipley SPR700(1.2). After the lithography process, the photoresist was irradiated by UV light using Fusion M150PC Photostabilizer to avoid photoresist deformation during the succeeding postbake. Postbake was done at 130 °C for 3 min and at 200 °C for 3 min on a hot plate. The waveguide pattern was transferred by a dry etching process [Fig. 3(c)]. The etching was done with an Applied Materials AME5300 using C_2F_6 17.9 sccm and CH_3F 12.1 standard cc/min (sccm) and source radio frequency and wafer biases of 1800 W and 470 W, respectively. Under these conditions, a high etch rate (-60 Å/s) was achieved and a high selectivity over photoresist (> 3) and a high aspect ratio were also achieved because CH_3F works as a sidewall protection layer due to its high carbon ratio. The obtained sidewall angle of air trench is 86°. Then wafers were cleaned by oxygen plasma ashing and piranha cleaning. Top cladding SiO_2 was deposited also by PECVD [Fig. 3(d)]. Chemomechanical polishing was applied to obtain a smooth surface for the second lithography

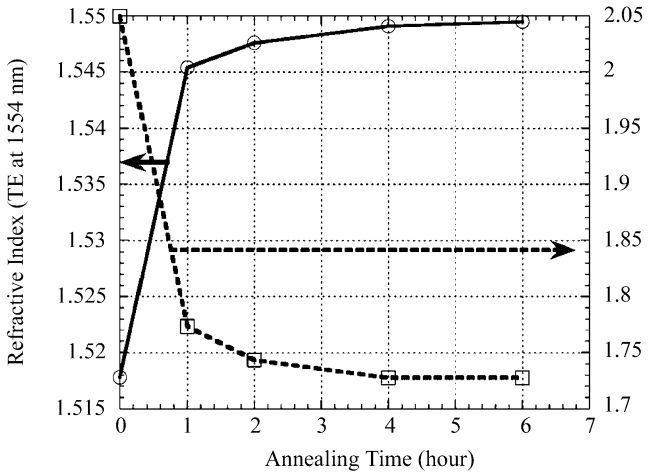

Fig. 4. Refractive index and thickness changes of the PECVD SiON after annealing (1554 nm TE mode). The refractive index increases by 0.033 and the thickness decreases by 15.7% as a result of consolidation annealing.

step by Strasbaugh Harmony 6EC [Fig. 3(e)]. A second photolithography and a dry etching step were performed to fabricate the air trench using the same procedure as for waveguide fabrication [Fig. 3(g)–(h)].

Fig. 5(a) and (b) shows a set of optical microscope top view images of an AT bend and a T-splitter where the radius is 10.7 μm and the taper angle is 80°. It can be seen that the two layers (waveguide and air trench layers) are well aligned with each other. Fig. 5(b) shows a set of scanning electron microscope (SEM) pictures of the AT bend and T-splitter. Table I summarizes the fabrication results in terms of dimensions realized in this process. The fabricated waveguides are close to design value and dimensions were obtained by SEM analysis.

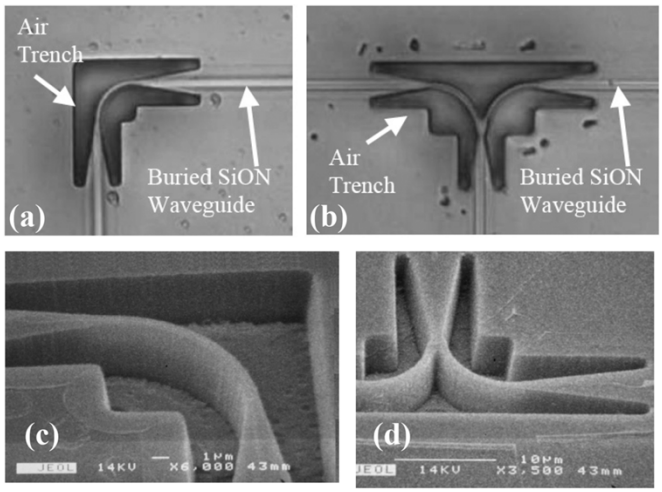

Fig. 5. Images of the fabricated structures. Optical microscope images: (a) AT bend and (b) T-splitter. SEM images: (c) AT bend (6000×) and (d) AT T-splitter (3500×).

TABLE I
POWER DISTRIBUTION RATIOS BETWEEN RIGHT AND LEFT ARMS FOR TM AND TE MODES. THE WAVELENGTH RANGES FROM 1540 TO 1560 nm. POWER SPLITTING RATIOS FOR BOTH TM AND TE MODES ARE AROUND 45:55. THE EXPECTED MISALIGNMENT BETWEEN WAVEGUIDE AND LAYERS IS 0.1 μm

AT Splitting Performance Power Splitting Ratio (percent)		
	Left Arm	Right Arm
TM	53.9 ± 5	46.1 ± 5
TE	54.5 ± 5	45.5 ± 5

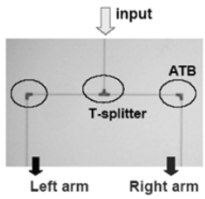

VI. MEASUREMENT RESULTS

Waveguide loss measurements were done using the Fabry–Pérot resonance method. Compared with the conventional cut-back method, this technique provides more precise measurement because optical contrast $(I_{\max}/I_{\min})$ does not depend on the coupling condition between optical fiber and waveguide, which is very sensitive to alignment conditions [7], [19]. The loss is simply calculated from the ratio of maximum to minimum intensity according to

$$\alpha = -\frac{1}{L}\ln\left(\frac{1}{R}\frac{\sqrt{\frac{I_{\max}}{I_{\min}}}-1}{\sqrt{\frac{I_{\max}}{I_{\min}}}+1}\right)$$

where α (cm^{-1}) is the propagation loss coefficient, L is the length of the waveguide, and R is the facet modal reflectivity. $I_{\max}$ and $I_{\min}$ are the peak and bottom intensities of the Fabry–Pérot spectrum, respectively. The reflectivity R was calculated by a three-dimensional (3-D) finite-difference time-domain (FDTD) simulation. The input and output facets were polished using a Buehler ECOMET3 system to suppress scattering at facets during measurement.

For both TE and transverse magnetic (TM) modes, this waveguide shows propagation loss as low as 0.27 ± 0.1 dB/cm. Loss was obtained by averaging the results from ten peaks and valleys in the Fabry–Pérot spectrum near 1550 nm.

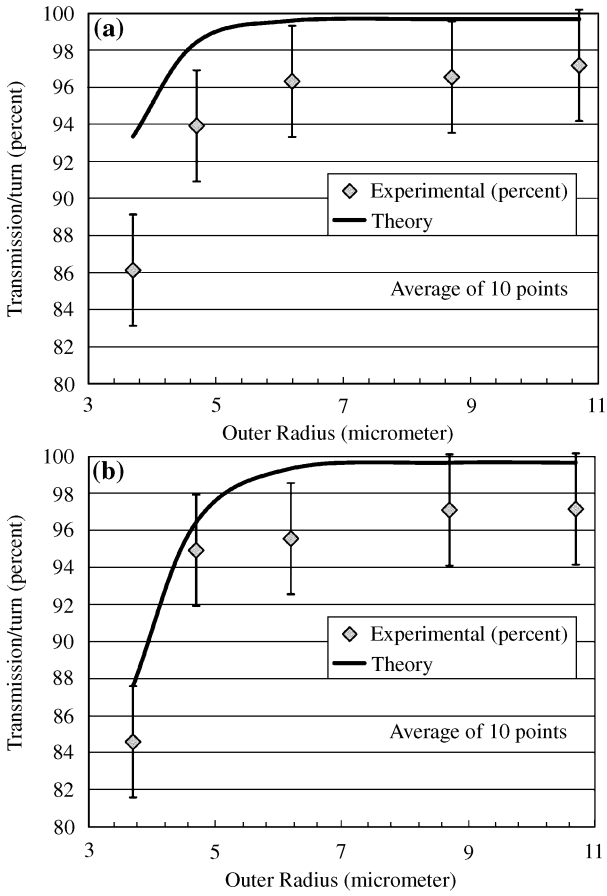

Fig. 6. Bending loss for ATB using (a) the TM mode and (b) the TE mode. Outer radii are varied from 3.7 to 10.7 μm. The taper angle is fixed at 80°. Experimental results are in good agreement with theoretical curves for transmission, as shown.

A. ATB Results

Fig. 6(a) and (b) shows bend losses for a 90° AT bend for TM ("quasi-TE" in [18], out-of-plane) and TE ("quasi-TM" in [18], in-plane) modes, respectively. The cladding taper angle is fixed at 80°, and the radii of the bend section are varied from 3.7 to 10.7 μm. Bend loss is as small as 0.1 dB/turn and matches to a reasonable degree the two-dimensional (2-D) FDTD simulation results for both polarizations. The geometry of air trenches is very well suited to approximation by 2-D FDTD using the effective index method [18]. However, the experimental results have as much as ∼0.15-dB standard deviation. The values shown in Fig. 6(a) and (b) are the averages of ten Fabry–Pérot resonance points near 1550 nm.

Another important factor for the miniaturization of bends while maintaining low loss is the cladding taper angle. Larger taper angles result in lower reflection and radiation losses, but increase device size. Finding an adequate taper angle is key to achieving compact low-loss bends. Fig. 7(a) and (b) shows bending loss per 90° AT bend for TM (quasi-TE) and TE (quasi-TM) modes, respectively, for several taper angles

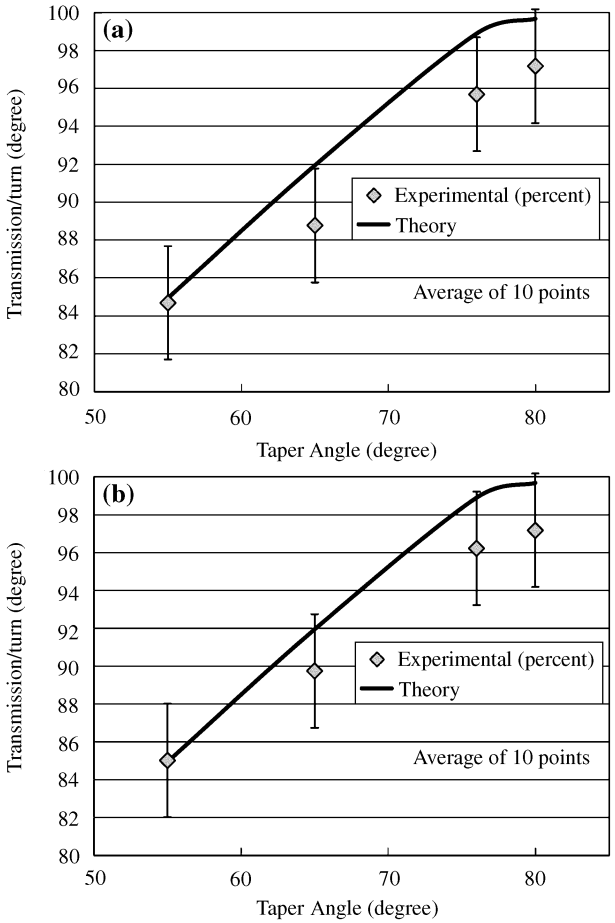

Fig. 7. Bending loss for ATB using (a) the TM mode and (b) the TE mode. Taper angle is varied from 55° to 80°. Experimental results are in good agreement with theoretical curves for transmission, as shown.

with the radius fixed at 10.7 μm. Experimental results match the simulation with some deviation. From these results, it is confirmed that the taper design has a significant impact on the bend loss as predicted from the theoretical simulation and that cladding tapers permitting low-loss bends can be fabricated.

B. Air Trench T-Splitter Results

In the T-splitter illustrated in Fig. 1(c) and shown in Fig. 5(b) and (d), the radius and taper angle are fixed at 10.7 μm and 80°, respectively. A straight throughput loss measurement was employed to find approximately less than 0.6-dB loss per junction. A key factor in T-splitters is even (or by design controllable) power distribution. Even power splitting is particularly important for optical clock distribution. Table I gives the measured power distribution for TM (quasi-TE) and TE (quasi-TM) modes. The splitting ratio for the device shown is approximately 45:55 for both TM and TE modes in the 1540- to 1565-nm wavelength range.

It was found that accurate alignment between the two structures (waveguide core and air trench structures) is an important factor for even power distribution. The splitting ratio was degraded to 30:70 when there is 0.3 μm lateral misalignment between the waveguide layer and the air trench layer. By paying attention to precise alignment, compact, low-loss, and even-power-splitting T-splitters can be realized using AT bends.

VII. Discussion and Summary

We presented the realization of novel waveguide structures by which sharp bend radii and dense integration can be achieved in low index contrast waveguides while keeping propagation loss and radiation (bend) loss within acceptable bounds. By introducing local high index contrast (the air trench) at the bend gradually, away from the core first, in a configuration that allows for adiabatic mode transition from low to high index contrast regions, a dramatic reduction in the bend radius of otherwise low index contrast waveguides is possible without causing large junction losses through mode mismatch and Fresnel reflection. This air trench technique can be applied to various kinds of index contrast systems ranging from $\Delta = 0.7\%$ (current PLC technology) to $\Delta = 20\%$ (high refractive index SiON) depending on future demands just by placing an air trench at the bend. We have demonstrated that this is a promising technique to achieve a compact waveguide system using current well-established CMOS technology. The results match theoretical simulations. The larger deviation from the theory (Figs. 6 and 7) at smaller radii and larger taper angles can be explained by scattering loss at bends and cladding tapers. At bends and tapers, the waveguide experiences local high index contrast and scattering loss becomes a more dominant loss source due to larger index difference.

The total bend length (radius and taper) was reduced by a factor of 5–50 in our silica examples depending on the index contrast. Because bend radius is one of the primary factors limiting the integration density in silica-based PLCs, the use of AT bends such as the ones presented here will allow dense integration leading to reduced cost and better yield while preserving the good fiber coupling and propagation loss properties associated with silica PLCs.

We also showed an AT T-splitter as a simple and compact splitter. In this case, precise alignment is required although it is achievable using the currently available exposure system.

Acknowledgment

Use of the NPACI Cray T-90 supercomputer at SDSC for finite-difference time-domain (FDTD) simulations is gratefully acknowledged. S. Akiyama would also like to thank C. Manolatou for the use of her well-written FDTD simulation code and the Microsystems Technology Laboratory, Massachusetts Institute of Technology, for providing the authors with useful fabrication techniques and useful discussions.

References

[1] T. Miya, "Silica-based planar lightwave circuits: Passive and thermally active devices," *IEEE J. Sel. Topics Quantum Electron.*, vol. 6, no. 1, pp. 38–45, Jan. 2000.

[2] E. A. J. Marcatili, "Bends in optical dielectric waveguides," *Bell Sys. Tech. J.*, vol. 48, no. 7, pp. 2103–2132, Sep. 1969.

[3] M. Heiblum and J. H. Harris, "Analysis of curved optical waveguides by conformal transformation," *IEEE J. Quantum Electron.*, vol. QE-11, no. 2, pp. 75–83, Feb. 1975.

[4] D. Rowland, "Nonperturbative calculation of bend loss for a pulse in a bent planar waveguide," *IEE Proc., Optoelectron.*, vol. 144, no. 2, pp. 91–96, Apr. 1997.
[5] I. C. Goyal, R. L. Gallawa, and A. K. Ghatak, "Bent planar waveguides and whispering gallery modes: A new method of analysis," *J. Lightw. Technol.*, vol. 8, no. 5, pp. 768–774, May 1990.
[6] M. K. Smit, E. C. M. Pennings, and H. Blok, "A normalized approach to the design of low-loss optical waveguide bends," *J. Lightw. Technol.*, vol. 11, no. 11, pp. 1737–1742, Nov. 1993.
[7] K. K. Lee, D. R. Lim, L. C. Kimerling, J. Shin, and F. Cerrina, "Fabrication of ultralow-loss Si/SiO_2 waveguides by roughness reduction," *Opt. Lett.*, vol. 26, no. 23, pp. 1888–1890, 2001.
[8] K. K. Lee, D. R. Lim, H.-C. Luan, A. Anu, J. Foresi, and L. C. Kimerling, "Effect of size and roughness on light transmission in a Si/SiO_2 waveguide: Experiments and model," *Appl. Phys. Lett.*, vol. 77, no. 11, pp. 1617–1619, 2000.
[9] M. Loncar, T. Doll, J. Vuckovic, and A. Scherer, "Design and fabrication of silicon photonic crystal optical waveguides," *J. Lightw. Technol.*, vol. 18, no. 10, pp. 1402–1411, Oct. 2000.
[10] A. Chuntinan and S. Noda, "Waveguides and waveguide bends in two-dimensional photonic crystal slabs," *Phys. Rev., B*, vol. 62, no. 7, pp. 4488–4492, 2000.
[11] A. Talneau, L. L. Gouezigou, N. Bouadma, M. Kafesaki, C. M. Soukoulis, and M. Agio, "Photonic-crystal ultrashort bends with improved transmission and low reflection at 1.55 μm," *Appl. Phys. Lett.*, vol. 80, no. 4, pp. 547–549, 2002.
[12] R. Germann, H. W. Salemink, R. Beyeler, G. L. Bona, F. Horst, I. Massarek, and B. J. Offrein, "Silicon oxynitride layers for optical waveguide applications," *J. Electrochem. Soc.*, vol. 147, no. 6, pp. 2237–2241, 2000.
[13] R. M. de Ridder, K. Worhoff, A. Driessen, P. V. Lambeck, and H. Albers, "Silicon oxynitride planar waveguiding structures for application in optical communication," *IEEE J. Sel. Topics Quantum Electron.*, vol. 4, no. 6, pp. 930–937, Nov.–Dec. 1998.
[14] A. del Prado, I. Martil, M. Fernandez, and G. Gonzalez-Diaz, "Full composition range silicon oxynitride films deposited by ECR-PECVD at room temperature," *Thin Solid Films*, vol. 343–344, no. 1, pp. 437–440, 1999.
[15] C. M. M. Denisse, K. Z. Troost, F. H. P. M. Habraken, W. F. van der Weg, and M. Hendriks, "Annealing of plasma silicon oxynitride films," *J. Appl. Phys.*, vol. 60, no. 7, pp. 2543–2547, 1986.
[16] D. Peters, K. Fischer, and J. Muller, "Integrated optics based on silicon oxynitride thin films deposited on silicon substrates for sensor applications," *Sens. Actuators, A, Phys.*, vol. 26, no. 1–3, pp. 425–431, 1991.
[17] K. Worhoff, A. Driessen, P. V. Lambeck, L. T. H. Hilderink, P. W. C. Linders, and T. J. A. Popma, "Plasma enhanced chemical vapor deposition silicon oxynitride optimized for application in integrated optics," *Sens. Actuators, A, Phys.*, vol. 74, no. 1–3, pp. 9–12, 1999.
[18] M. Popovic, K. Wada, S. Akiyama, H. A. Haus, and J. Michel, "Air trenches for sharp silica waveguide bends," *J. Lightw. Technol.*, vol. 20, no. 9, pp. 1762–1772, Sep. 2002.
[19] A. Sakai, G. Hara, and T. Baba, "Propagation characteristics of ultra-high-Δ optical waveguide on silicon-on-insulator substrate," *Jpn. J. Appl. Phys.*, vol. 40, no. 4B, pp. L383–L385, 2001.

Shoji Akiyama (S'03) received the B.S. and M.S. degrees in chemistry from Kyoto University, Kyoto, Japan, in 1995 and 1997, respectively. He is currently working toward the Ph.D. degree at MIT, pursuing microphotonics as his research topic.

In 1997, he joined Shin-Etsu Chemical Company, Ltd., Chiyoda-ku, Tokyo 100-0004. In 2000, he entered Prof. L. C. Kimerling's group at the Department of Materials Science and Engineering, Massachusetts Institute of Technology (MIT), Cambridge.

Miloš A. Popović (S'98) was born in Zajecar, Yugoslavia, on 1977. He received the B.Sc. degree in electrical engineering from Queen's University, Kingston, ON, Canada, in 1999, and the M.S. degree from the Massachusetts Institute of Technology (MIT), Cambridge, in 2002. He is currently working toward the Ph.D. degree at MIT, pursuing integrated optics as his research topic.

Peter T. Rakich was born in Hinsdale, IL, on 1976. He received the B.S. degree in physics from Purdue University, Lafayette, IN, in 1999. He is currently working toward the Ph.D. degree in physics from the Massachusetts Institute of Technology, Cambridge, researching photonic devices and integrated optics.

Kazumi Wada received the B.S. and M.S. degrees and the Ph.D. degree in instrumentation engineering from Keio University, Yokohama, Japan, in 1973, 1975, and 1982, respectively.

Since joining NTT Laboratories, Tokyo, Japan, in 1975, he has been engaged in research on defects in silicon and III–V semiconductor materials and devices, including oxygen precipitation kinetics in Si. From 1981 to 1982, he was a Visiting Scientist at the Massachusetts Institute of Technology (MIT), Cambridge, conducting research on defects in GaAs. From 1982 to 1983, he was a Visiting Specialist at the Science and Technology Agency of the Japanese Government working on establishing a guideline on semiconductor materials research in Japan. Since 1998, he has been with the MIT Microphotonics Center, Department of Materials Science and Engineering, conducting research on silicon-based photonic integrated circuits. His current interest is on-chip optical interconnection for high-speed Si-LSIs. He has authored and coauthored more than 100 refereed journal papers and has edited 13 books. He is an Associated Editor of the *Japanese Journal of Applied Physics.*

He is an active Member of the Materials Research Society, the Electrochemical Society, and the Japan Society of Applied Physics. Dr. Wada has been serving as an Associate Editor of the IEEE/The Minerals, Metals & Materials Society JOURNAL OF ELECTRONIC MATERIALS.

Jürgen Michel received the diploma in physics from the University of Cologne, Cologne, Germany, in 1983, and the Ph.D. degree in applied physics from the University of Paderborn, Germany, in 1987.

He was a Research Scientist at the University of Paderborn. Prior to joining the Massachusetts Institute of Technology (MIT), Cambridge, in 1990, he was a Postdoctoral Member of the Technical Staff at AT&T Bell Laboratories, Holmdel, NJ, studying defect reactions and defect properties in semiconductor materials. He is currently a Principal Research Associate at the Microphotonics Center in MIT. He manages and conducts research projects on silicon-based photonic materials and devices and contamination issues in silicon processing. His main focus is currently on optical-clock distribution and coupling and packaging issues in microphotonics and on-chip WDM devices. He has authored and coauthored more than 80 technical articles.

Hermann A. Haus (S'50–A'55–SM'58–F'62–LF'91) was born in Ljubljana, Slovenia, on 1925. He attended the Technische Hochschule, Graz, and the Technische Hochschule, Vienna, Austria. He received the B.Sc. degree from Union College, Schenectady, NY, in 1949, the M.S. degree from the Rensselaer Polytechnique Institute, Troy, NY, in 1951, and the Sc.D. degree from the Massachusetts Institute of Technology (MIT), Cambridge, in 1954.

He joined the Faculty of Electrical Engineering at MIT in 1954, where he is an Institute Professor. He is engaged in research on electromagnetic theory and lasers. He has authored and coauthored six books and more than 360 journal articles.

Dr. Haus is a Fellow of the American Physical Society and the Optical Society of America (OSA) and a Member of the National Academy of Engineering, the National Academy of Sciences, and the American Academy of Arts and Sciences. He is the recipient of the 1984 Award of the Institute of Electrical and Engineers (IEEE) Quantum Electronics and Applications Society, the 1987 Charles Hard Townes Prizes of the (OSA), the 1991 IEEE Education Medal, the 994 Frederic Ives medal, the Ludwig Wittgenstein-Preis Award of the Austrian Government 1997, and the Willis E. Lamb medal 2001. He holds honorary doctorate degrees from Union College, the Technical University of Vienna, Austria, and the University of Ghent, Belgium.

Erich P. Ippen (S'66–M'69–SM'81–F'84) received the S.B. degree in electrical engineering from the Massachusetts Institute of Technology (MIT), Cambridge, in 1962 and the M.S. and Ph.D. degrees in electrical engineering from the University of California, Berkeley, in 1965 and 1968, respectively.

He was a Member of the Technical Staff at Bell Laboratories, Holmdel, NJ, from 1968 to 1980. In 1980, he joined the faculty of MIT, where he is currently the Elihu Thomson Professor of Electrical Engineering and Professor of Physics. His research interests include nonlinear optics in fibers, femtosecond pulse generation, ultrafast processes in materials and devices, photonic bandgap structures, and ultrashort-pulse fiber devices.

Prof. Ippen is a Fellow of the American Physical Society and the Optical Society of America (OSA). He is a Member of the National Academy of Sciences, the National Academy of Engineering, and the American Academy of Arts and Sciences.

Lionel C. Kimerling (M'89) received the S.B. degree in metallurgical engineering and the Ph.D. degree in materials science from the Massachusetts Institute of Technology (MIT), Cambridge, in 1965 and 1969, respectively.

He was formerly Head of the Materials Physics Research Department, AT&T Bell Laboratories, Holmdel, NJ. He is presently the Thomas Lord Professor of Materials Science and Engineering at MIT. In addition to his teaching duties in electronic, optical, and optoelectronic materials, he is the Director of the MIT Materials Processing Center. His current research is on silicon processing addresses, photovoltaic cells, environmentally benign integrated circuit manufacturing, and monolithic microphotonic devices and circuits.